Volume Integral Equations for Electromagnetic Scattering from Dielectric Objects: Observations and Questions

Andrew F. Peterson
School of Electrical and Computer Engineering
Georgia Institute of Technology, Atlanta, GA 30332-0250
(Email: peterson@ece.gatech.edu)

***Abstract*—Five volumetric formulations for electromagnetic scattering from dielectric bodies modeled with tetrahedral cells are evaluated to compare their performance. For test problems, all five approaches produce solutions for scattering cross section and internal fields that converge to the correct results. Some formulations are far more efficient than others, however. A point-tested version of the popular Galerkin EFIE-D approach is shown to be similar in far field accuracy to the more expensive Galerkin formulation.**

***Index Terms*—Method of Moments (MoM), Numerical Techniques, Solenoidal Basis Functions, Tetrahedral Cells, Volume Integral Equations**

I. Introduction and A Brief History

Electromagnetic scattering from heterogeneous dielectric bodies has been of interest to the computational community since the 1960s. Early 3D techniques were based on the volume electric-field integral equation (EFIE) discretized using "block" models of the target [1-2]. These schemes employed what we now know as an "EFIE-J" formulation, where the polarization current *J* is directly expanded in basis functions (usually piecewise constant or "pulse" functions). Here we focus our attention on approaches that employ tetrahedral cells, with a permittivity function that is constant within each cell. The first tetrahedral-cell formulation was proposed in the early 1980s [3], and employed face-based "constant normal–linear tangential" mixed-order divergence-conforming basis functions (which became known as Schaubert-Wilton-Glisson functions) to represent the electric flux density, thus imposing the proper discontinuity of the normal electric field at jump discontinuities in permittivity. This scheme is known as an "EFIE-D" formulation. With scaling, the Galerkin-tested EFIE-D approach of [3] produces a symmetric system matrix and has probably been the most widely used formulation for heterogeneous dielectric targets.

A 3D magnetic field integral equation (MFIE) formulation was proposed in 1989 [4]. That approach employed a node-based linear expansion of the vector magnetic field on tetrahedrons, and will be denoted by the label "MFIE-N" in the following examples. The scheme of [4] involved a solenoidal electric flux density that eliminated fictitious volume charge densities and also produces the proper normal electric field discontinuity at material boundaries. While the MFIE does not generate a symmetric system of equations, the point-tested version eliminates the need for any volumetric integrals, and the approach requires far fewer unknowns for a given mesh than the EFIE-J or EFIE-D formulations. The primary drawback of the MFIE-N approach is the lack of generality in the expansion; because of the scalar Lagrangian basis functions the normal component of the magnetic field is not able to jump at a cell boundary, preventing the formulation from being able to simultaneously handle dielectric and magnetic materials.

Solenoidal basis functions on tetrahedrons were first used within the EFIE to represent the electric flux and eliminate fictitious charge density in a 1999 paper [5]. The representation is equivalent to expanding the *H*-field in the "constant tangential–linear normal" (CT/LN) mixed-order curl-conforming basis functions, and computing the *D*-field by taking the curl of *H*. Thus, we refer to it as the "EFIE-H" approach. In common with the point-tested MFIE-N formulation, this (Galerkin) approach can be implemented with no volume integrations [6]. The EFIE-H approach requires fewer unknowns for the same mesh than the EFIE-J or EFIE-D. The solenoidal space extracted from the CT/LN functions is not linearly independent, and some additional preprocessing is required to identify a linearly independent subspace [7].

In a 2006 paper [8], the 3D MFIE was discretized using edge-based curl-conforming basis functions for *H*, which also produce a solenoidal electric flux density, and the proper normal *D*-fields at dielectric interfaces. We refer to this approach as the "MFIE-H" formulation. The lowest-order basis considered in [8] was the curl-conforming CT/LN functions, which were subsequently shown to fail [9] for large values of permittivity. However, the "linear tangential–linear normal" (LT/LN) mixed-order curl-conforming basis functions, also used in [8-9], are

demonstrated below to produce accurate, stable solutions. In addition, they may be implemented with only one unknown per edge, as discussed in Section IV.

The preceding EFIE formulations employ divergence-conforming basis functions that impose normal-vector continuity of the electric flux across faces of the mesh. A distinctly different EFIE approach was proposed in 2009 [10] that uses an edge-based expansion of the internal electric field in terms of curl-conforming CT/LN vector basis functions. Thus, this is an "EFIE-E" formulation. The CT/LN functions maintain the tangential-vector continuity of the electric field across faces of the mesh. Since there is one unknown per edge of the mesh, the approach requires fewer unknowns for a given 3D mesh than the face-based expansion of [3], but not as few as the EFIE-H or MFIE-N formulations.

EFIE-J formulations have received recent attention for tetrahedral models [11-12]. These usually employ piecewise constant representations for the polarization current and electric fields, and do not impose continuity of either the normal flux or the tangential fields. They require substantially more unknowns for a given mesh than the other approaches under consideration.

In summary, four EFIE and three MFIE formulations have been proposed. References [8] and [9] have evaluated several of these, but only in terms of their far fields. In the following, we provide numerical results to compare the performance of three EFIE and two MFIE formulations, and discuss their relative efficiency for dielectric targets. The error in the scattering cross section and internal fields will be used to judge the performance. Details of each approach may be found in the literature, with the major features of each summarized in Section II.

II. Relative Efficiency of Expansions

The choice of optimal type of unknown may be guided by the growth rate of various parameters (edges, faces, etc.) in a large tetrahedral mesh. There are two well-known schemes for dividing a brick or hexahedron into 5 or 6 tetrahedrons [13]. Table I summarizes the rate of growth of cells, faces, and edges as a function of the number of nodes based on these schemes. Although this approach (starting with bricks and subdividing) is not typically employed by mesh generators to tessellate volumes, the resulting numbers are close to the growth rates observed for actual meshes. Table I also shows the growth rate of the number of faces minus the number of cells, which is the asymptotic rate associated with the linearly independent subspace of the solenoidal divergence-conforming representation.

Table II shows estimates of the number of unknowns required from each approach for a large tetrahedral mesh, based on the asymptotic growth rates in Table I. The cell-based expansion (EFIE-J) requires three unknowns per cell, while the node-based expansion requires three unknowns per node. Edge-based and face-based expansions require one unknown per edge and face, respectively. The solenoidal approach (EFIE-H) involves a linearly independent subspace that grows in proportion to the number of faces minus the number of cells.

Table I

Asymptotic estimates for the number of cells, edges, etc. in a large tetrahedral mesh as a function of the number of nodes. Based on the division of a brick mesh into tetrahedrons.

nodes	N
cells	~5N–6N
edges	~6N–7N
faces	~10N–12N
faces – cells	~5N–6N

From Table II, it is apparent that the number of unknowns varies considerably depending on the method. The EFIE-J formulation requires approximately 5 times as many unknowns as the MFIE-N formulation for the same mesh. However, relative performance must also take into account the accuracy produced by each formulation.

III. Performance of Galerkin-tested Formulations

In this section the relative accuracy of the EFIE-D, EFIE-E, EFIE-H, MFIE-N, and MFIE-H LT/LN approaches will be investigated. All results will be obtained for Galerkin-tested formulations (using the same functions to enforce the equation as are used to represent the principal unknown). Galerkin testing produces a symmetric system of equations for the EFIE formulations and is sometimes associated with a superconvergence in the far field [14]. Testing integrals were implemented using an 11-point Gauss rule for tetrahedrons. Inner integrals were performed using adaptive quadrature and singularity cancellation procedures to handle the Green's function singularity. We do not include the MFIE-H CT/LN in this comparison since that approach fails in our tests, as previously observed [9].

Results are presented for scattering problems involving homogeneous, spherical dielectric targets, and one layered dielectric sphere. EFIE results for other targets have been provided in [6]. For the homogeneous sphere targets, a series of tetrahedral-cell meshes was created with the properties displayed in Table III.

The first example involves a homogenous lossy sphere, with $ka = 1$ and $\varepsilon_r = 4 - j3$. For the series of models under consideration, the average cell edge length in each model is shown in Table III. Figure 1 shows the error in the scattering cross section (SCS) σ obtained with the five formulations. The error in σ is computed from the expression

$$E = \frac{\sqrt{\dfrac{1}{N_{angles}} \sum_{n=1}^{N_\theta} \sum_{m=1}^{N_\phi} \sin\theta_m \left| \sigma_{exact}(\theta_m, \phi_n) - \sigma_{num}(\theta_m, \phi_n) \right|^2}}{\sigma_{exact}(\theta_{forward}, \phi_{forward})} \quad (1)$$

Table II

Estimated number of unknowns for each approach applied to a large mesh with N nodes, and an indication of whether the formulation can be implemented with Galerkin testing and with point testing.

approach	basis	unknowns	Galerkin test	Point test
EFIE-J	pulse for x, y, z	~15N–18N	Yes	Yes
EFIE-D	SWG	~10N–12N	Yes	Yes
EFIE-E	CT/LN	~6N–7N	Yes	?
EFIE-H	Curl of CT/LN	~5N–6N	Yes	?
MFIE-N	linear Lagrangian	3N	Yes	Yes
MFIE-H	CT/LN	~6N–7N	Yes	Yes
MFIE-H	LT/LN	~12N–14N	Yes	Yes

Note: The MFIE-H LT/LN formulation can be implemented with one unknown per edge, cutting this estimate in half if additional matrix manipulations are used during matrix fill, as described in Section IV.

Table III.

Mesh characteristics for five sphere models.

cells	faces	edges	average edge length	average edge length	average edge length
			ka = 1, $\varepsilon_r = 4 - j3$	ka = 0.35 ε_r = 10	ka = 0.35 $\varepsilon_r = 40 - j10$
32	80	66	0.37 λ_d	0.18 λ_d	0.37 λ_d
203	451	310	0.22 λ_d	0.11 λ_d	0.22 λ_d
825	1752	1119	0.14 λ_d	0.069 λ_d	0.14 λ_d
1254	2672	1711	0.12 λ_d	0.059 λ_d	0.12 λ_d
3383	7067	4380	0.086 λ_d	0.042 λ_d	0.086 λ_d

Figure 2 shows the error in the internal fields obtained for the same target as Figure 1, for a uniform plane wave excitation. The field error is computed from the normal component of the electric field at the center of each face in each model, using the expression

$$E = \frac{1}{\varepsilon_r \eta_0} \sqrt{\frac{1}{N_{faces}} \sum_{n=1}^{N_{faces}} \left| \varepsilon_r E_n^{nor} \Big|_{exact} - \varepsilon_r E_n^{nor} \Big|_{num} \right|^2}. \quad (2)$$

We show the error in the normal electric field for all five techniques, even though this is only the primary unknown for the EFIE-D and EFIE-H formulations. The average value on either side of the face is used with the EFIE-E, which has a discontinuous normal E-field. The exact results for scattering cross section and internal fields are determined from the eigenfunction series (Mie series) solution of the sphere scattering problem. From Figures 1 and 2, the best errors on a per-unknown basis are those obtained with the EFIE-H and MFIE-N formulations.

As a second example, consider a lossless sphere with ka = 0.35 and ε_r = 10. Figures 3 and 4 show the error in the scattering cross section and internal electric fields, respectively, for the EFIE-D, EFIE-H, MFIE-N, and MFIE-H formulations. The four formulations produce similar error levels for the same meshes (especially for the internal electric fields); the primary difference in the plots is due to the different number of unknowns required by each approach. For this target, the MFIE-H CT/LN formulation (results not shown) exhibited large errors that did not decrease as the meshes were refined.

Next, we consider a very lossy sphere with ka = 0.35 and $\varepsilon_r = 40 - j\,10$. Figures 5 and 6 show the error obtained with the three EFIE and two MFIE approaches. Unlike the preceding examples, here the MFIE formulations produce steeper curves for the scattering cross section errors than the EFIE formulations. These slopes were steeper than typically observed with the MFIE. For this target, the MFIE-H CT/LN formulation (results not shown) exhibited large errors.

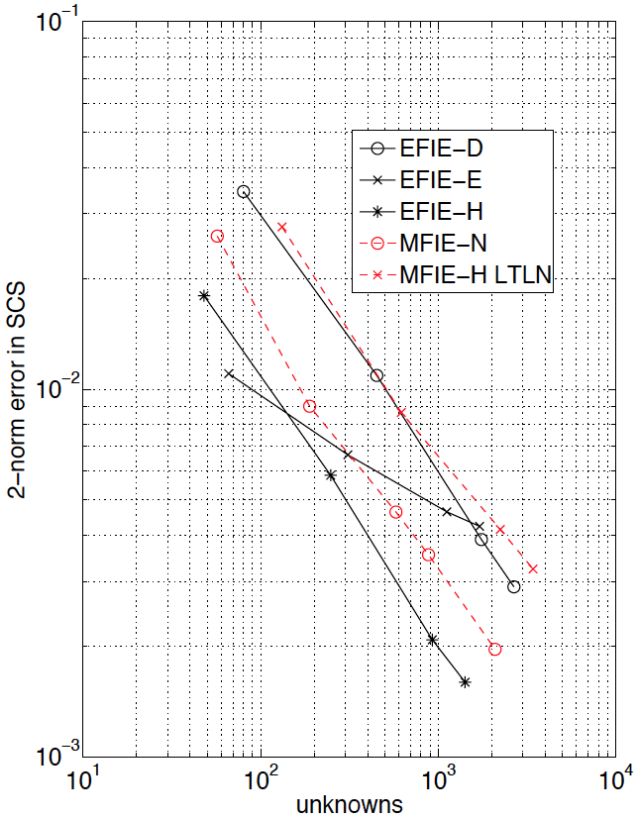

Fig. 1. The error in scattering cross section for a dielectric sphere with $ka = 1.0$ and $\varepsilon_r = 4 - j\,3$.

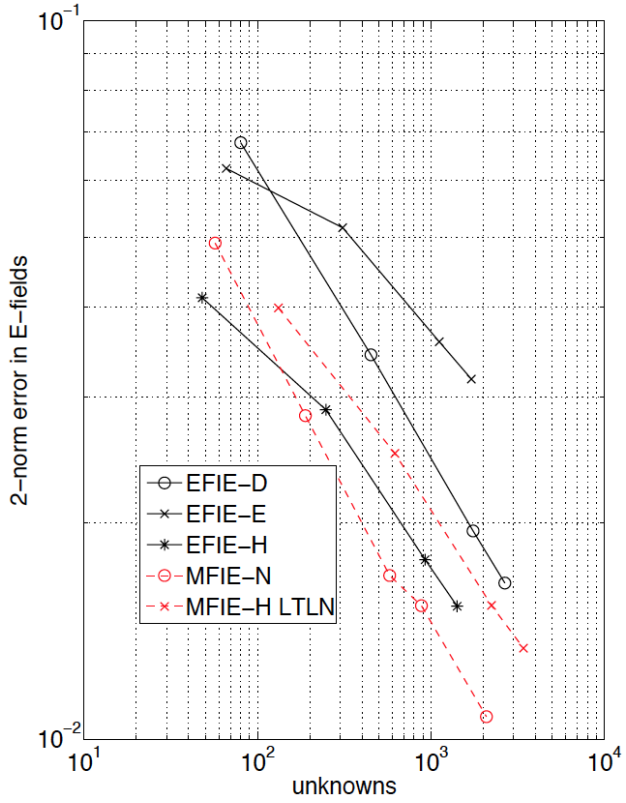

Fig. 2. The internal field error for a sphere with $ka = 1.0$ and $\varepsilon_r = 4 - j\,3$.

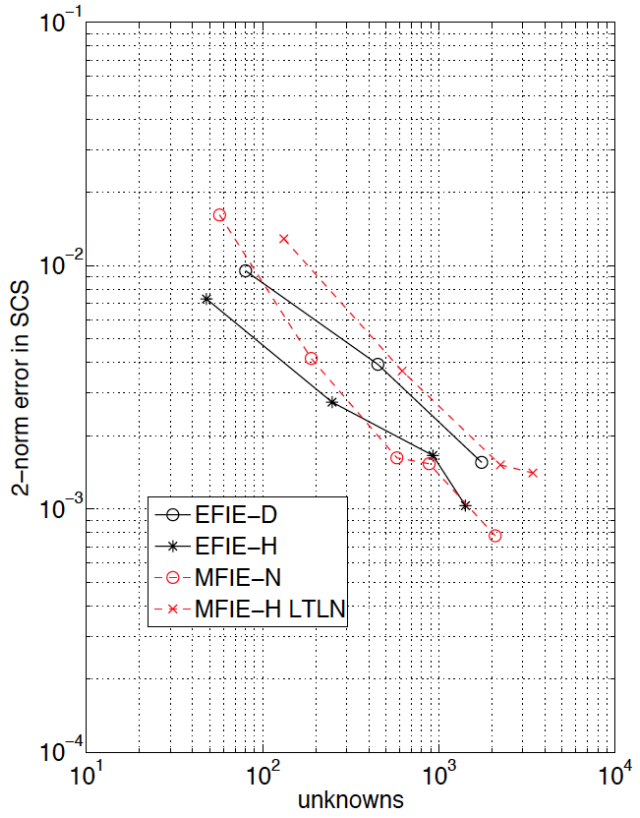

Fig. 3. The error in scattering cross section for a dielectric sphere with $ka = 0.35$ and $\varepsilon_r = 10$.

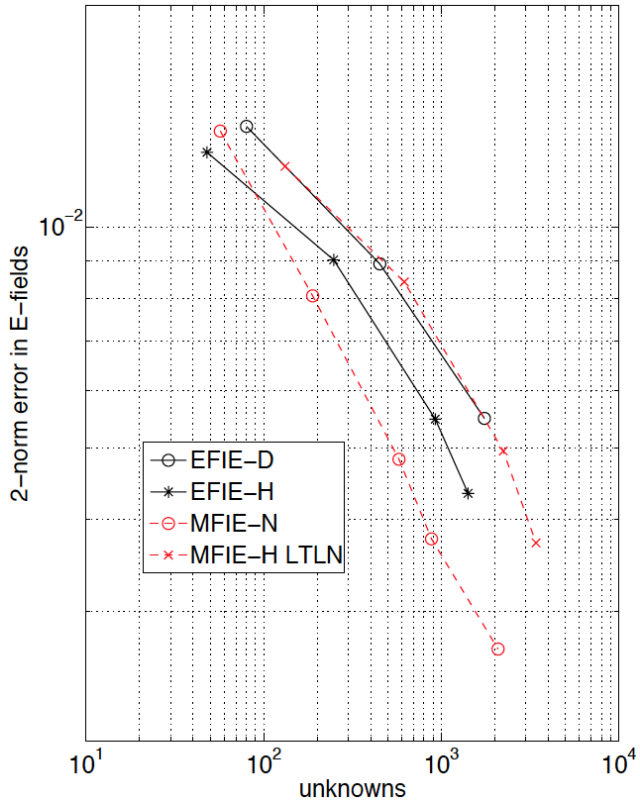

Fig. 4. The internal field error for a sphere with $ka = 0.35$ and $\varepsilon_r = 10$.

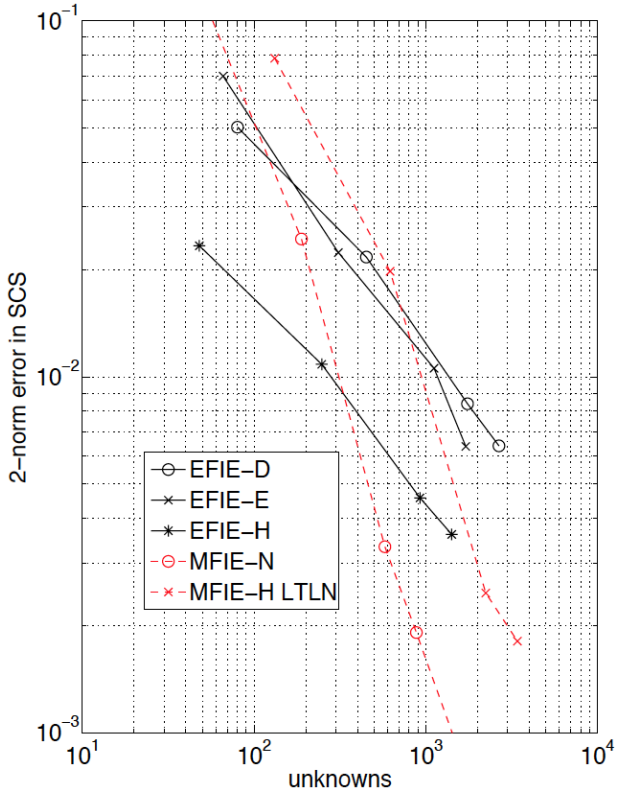

Fig. 5. The error in scattering cross section for a dielectric sphere with ka = 0.35 and ε_r = 40 – j 10.

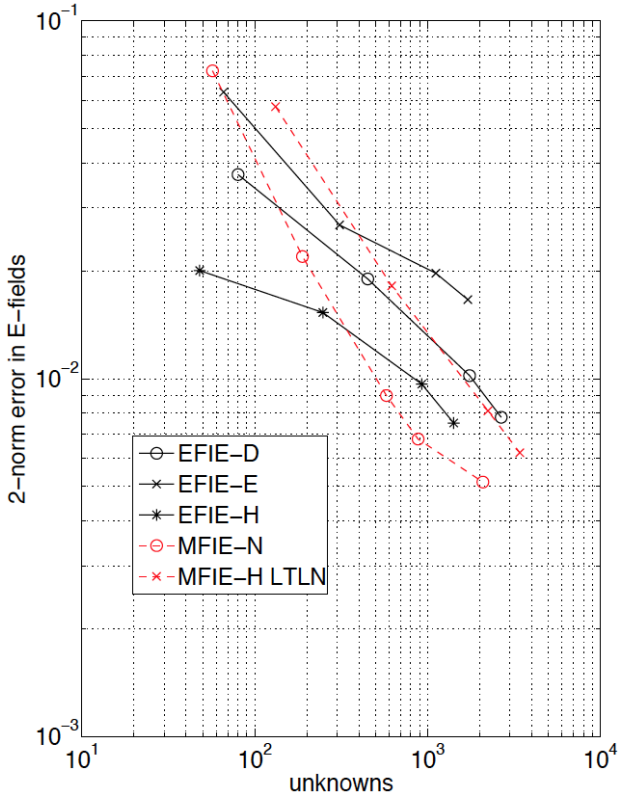

Fig. 6. The internal field error for a sphere with ka = 0.35 and ε_r = 40– j 10.

For almost all the examples considered, including those not reported here, the rate of error convergence for scattering cross section appears to be O($N^{2/3}$), where N is the number of unknowns, while that for the internal fields is approximately O($N^{1/3}$). These rates are equivalent to rates of O(h^2) and O(h) for the scattering cross section and internal fields, respectively, where h is the average edge length of the mesh. (There are occasional deviations from these rates. In Figure 1 the EFIE-E scattering cross section converged at a slower rate, while in Figure 5 both MFIE results converged at a faster rate.) A convergence rate of O(h) in the field error is expected for a piecewise-constant representation; all approaches ultimately use that representation for the electric field. The scattering cross section usually convergences at a rate of O(h^2) for all five techniques. Since this exceeds the rate of the internal fields and polarization current density, it is a superconvergent rate, as might be expected from Galerkin constructions [14].

The preceding examples all involved homogeneous targets. As our final example, consider a sphere with a core of ka = 0.625 and ε_r = 2, surrounded by a cladding of outer dimension kb = 1.0 and ε_r = 4. Three tetrahedral meshes were employed with 223, 734, and 2598 cells, respectively. Figures 7 and 8 show the error obtained with the five formulations, compared to reference solutions obtained from an eigenfunction expansion. The EFIE results were previously published in [6]. For the internal field error norm, we replace (2) by

$$E = \frac{1}{\varepsilon_{r,avg}\eta_0}\sqrt{\frac{1}{N_{faces}}\sum_{n=1}^{N_{faces}}\left|\varepsilon_r E_n^{nor}\Big|_{exact} - \varepsilon_r E_n^{nor}\Big|_{num}\right|^2} \qquad (3)$$

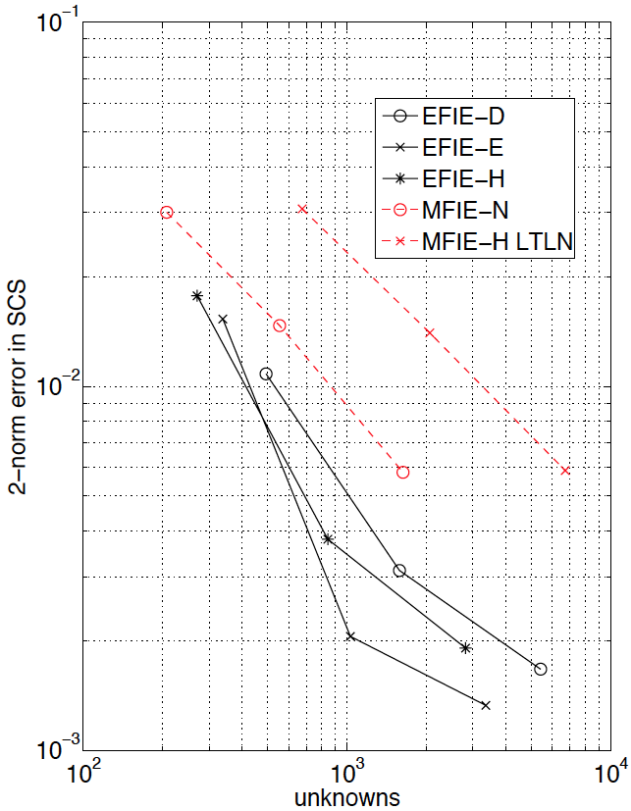

Fig. 7. The error in scattering cross section for a layered dielectric sphere with a core of ka = 0.625 and ε_r = 2, and a cladding of kb = 1.0 and ε_r = 4.

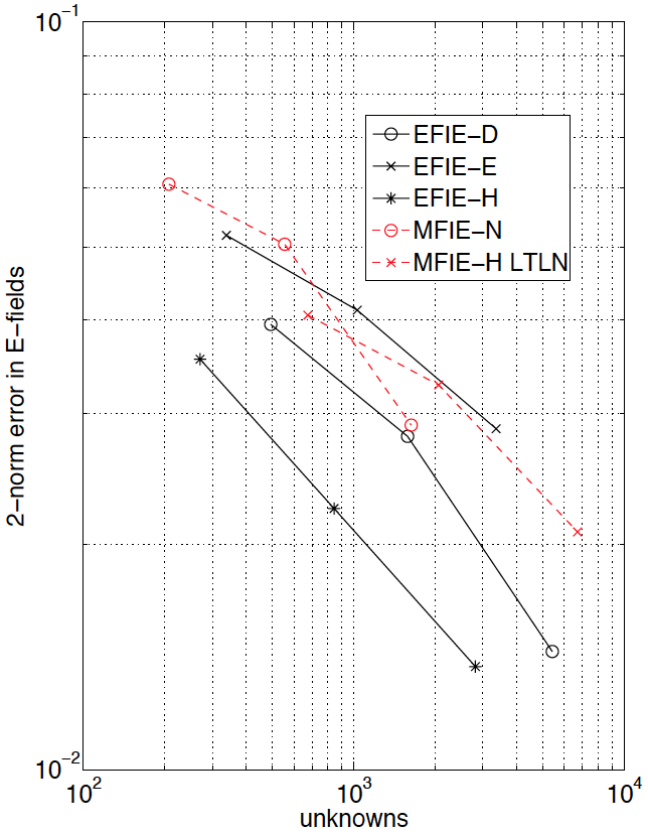

Fig. 8. The error in internal fields for a layered dielectric sphere with a core of ka = 0.625 and ε_r = 2, and a cladding of kb = 1.0 and ε_r = 4.

where the average relative permittivity ($\varepsilon_{r,avg}$ = 3) is used for the normalization. The behavior in Figure 7 is somewhat different from the preceding examples, in that the MFIE formulations produced relatively large SCS errors (almost identical for the two formulations for each mesh) while the EFIE-E produced the most accurate SCS values.

From an examination of the preceding figures, one observes that the accuracy of these five formulations is usually similar (often within a factor of two) for a given mesh, but appears quite different when plotted versus the number of unknowns. Thus, the comparison in Table II is relevant. The EFIE-H approach, which only requires about half the unknowns required by the EFIE-D formulation, is the most efficient EFIE formulation in terms of accuracy versus unknowns. The MFIE-N approach is comparable or better than the EFIE-H in most of these examples, but we note that the generality of the node-based expansion prevents the use of that formulation for problems where permeability is also varying. The relative execution times of these approaches are dominated by matrix fill times for these problem sizes. The EFIE-D approach involves the most complicated and costly integrals, while the EFIE-H requires no volume integrals and is consequently much cheaper. The MFIE codes only use volume integrations for the testing integrals (an 11-point Gauss rule for these results).

Another relevant aspect of this type of comparison is that of relative stability, as indicated by the matrix condition number of the formulations. A related metric is the convergence rate of iterative solvers. These issues have not been thoroughly studied to date by the author, and must be left for future investigations.

IV. Reduction of Unknowns with MFIE-H LT/LN

The preceding figures were plotted using twice the number of edges as the number of unknowns for the MFIE-H LT/LN formulation. However, due to the nature of the representation, the size of the system matrix can be reduced to half that value. The curl-conforming LT/LN basis functions consist of a subset of rotational functions, locally defined in terms of simplex coordinates (L_1,L_2,L_3,L_4) as

$$\bar{R}_{ij} = w_{ij}\left(L_i \nabla L_j - L_j \nabla L_i\right) \tag{4}$$

and a subset of irrotational functions, locally defined as

$$\bar{G}_{ij} = w_{ij}\left(L_i \nabla L_j + L_j \nabla L_i\right) \tag{5}$$

where w_{ij} is the edge length. Since the functions in (5) have zero curl, they produce no scattered magnetic field. As a result, the system matrix arising from Galerkin testing can be partitioned into the form

$$\begin{bmatrix} D_{RR} - Y_{RR} & D_{RG} \\ D_{GR} - Y_{GR} & D_{GG} \end{bmatrix} \begin{bmatrix} \alpha \\ \beta \end{bmatrix} = \begin{bmatrix} \langle \bar{R}_m, \bar{H}^{inc} \rangle \\ \langle \bar{G}_m, \bar{H}^{inc} \rangle \end{bmatrix} \tag{6}$$

where the various "D" blocks are sparse Gram matrices

$$D_{RRmn} = \langle \bar{R}_m, \bar{R}_n \rangle \tag{7}$$

$$D_{RGmn} = \langle \bar{R}_m, \bar{G}_n \rangle \tag{8}$$

$$D_{GRmn} = \langle \bar{G}_m, \bar{R}_n \rangle \tag{9}$$

$$D_{GGmn} = \langle \bar{G}_m, \bar{G}_n \rangle \tag{10}$$

and the full matrix blocks are the tested scattered H-fields due to the rotational functions,

$$Y_{RRmn} = \langle \bar{R}_m, \bar{H}^s \left\{ \frac{\varepsilon_r - 1}{\varepsilon_r} \nabla \times \bar{R}_n \right\} \rangle \tag{11}$$

$$Y_{GRmn} = \langle \bar{G}_m, \bar{H}^s \left\{ \frac{\varepsilon_r - 1}{\varepsilon_r} \nabla \times \bar{R}_n \right\} \rangle \tag{12}$$

In the above, the brackets denote a conceptual three-dimensional vector product

$$\langle \bar{R}_m, \bar{R}_n \rangle = \iiint \bar{R}_m \bullet \bar{R}_n \, dv \tag{13}$$

while $\bar{H}^s\{\bar{S}\}$ denotes the scattered H-field produced by the source function $\bar{S}$. Note that the scattered field calculations are implemented in such a way that the integrals collapse to cell faces, as described in [4,6].

Since the "D" matrices in (6) are sparse, the coefficients of the irrotational functions may be obtained from

$$\begin{aligned} [\beta] = &\left[D_{GG}\right]^{-1}\left[\langle \bar{G}_m, \bar{H}^{inc} \rangle\right] \\ &-\left[D_{GG}\right]^{-1}\left[D_{GR} - Y_{GR}\right][\alpha] \end{aligned} \tag{14}$$

and eliminated from the other equation, yielding a system

$$\left[\left(D_{RR}-Y_{RR}\right)-D_{RG}\left(D_{GG}\right)^{-1}\left(D_{GR}-Y_{GR}\right)\right][\alpha] = \left[\langle \bar{R}_m, \bar{H}^{inc}\rangle - D_{RG}\left(D_{GG}\right)^{-1}\langle \bar{G}_m, \bar{H}^{inc}\rangle\right] \quad (15)$$

with order equal to the number of edges in the mesh (half that of the original approach). The inverse matrix in (14) and (15) is a sparse matrix with approximately 14 nonzero entries per row. Therefore the inversion can be performed by sparse factorization using one of the standard procedures [15-18], at a cost far less than O(N^2).

A point-tested version of the MFIE-H LT/LN formulation may be realized with half the unknowns without the need for the matrix operations required by the Galerkin formulation in (14) and (15). Suppose that the point testing is done at two symmetric points on each edge, with points located a distance γ between the center of the edge ($\gamma = 0$) and the ends ($\gamma = \pm 1$). The new system has the form

$$\begin{bmatrix} I - Y_{+R} & \gamma I \\ I - Y_{-R} & -\gamma I \end{bmatrix}\begin{bmatrix} \alpha \\ \beta \end{bmatrix} = \begin{bmatrix} \hat{t}_{m+} \bullet \bar{H}^{inc} \\ \hat{t}_{m-} \bullet \bar{H}^{inc} \end{bmatrix} \quad (16)$$

where "I" denotes an identity matrix. The sum of the two block rows produces the system

$$\left[2I - Y_{+R} - Y_{-R}\right][\alpha] = \left[\hat{t}_{m+} \bullet \bar{H}^{inc} + \hat{t}_{m-} \bullet \bar{H}^{inc}\right]. \quad (17)$$

Thus, the system matrix for the point-matched version can be obtained with one unknown per edge by the simple task of superimposing the H-fields of the two types of basis functions in (4) and (5).

V. Point-Matched versus Galerkin Approaches

The EFIE-D and MFIE formulations can be implemented with point testing, raising the question of whether or not there is an advantage to the (more expensive) Galerkin testing procedure often employed. To explore this possibility, we generated results for point-tested versions of the previous formulations. The other EFIE formulations considered previously, EFIE-E and EFIE-H, are inherently Galerkin and not amenable to point testing.

Figures 9 and 10 show the error in the scattering cross section and internal electric fields, respectively, produced by the point-tested and Galerkin-tested EFIE-D and MFIE-H LT/LN formulations, for a sphere with ka = 1.0 and ε_r = 5. Figures 11 and 12 show similar results for a sphere with ka = 0.35 and $\varepsilon_r = 40 - j\,10$. Because the point-tested MFIE-H formulation (equation 17) is trivial to implement with one unknown per edge, we use the smaller unknown count for the point-tested MFIE-H but use two unknowns per edge for the Galerkin-tested MFIE-H. We observed varying accuracy in the point-tested MFIE as the test point locations were adjusted along the cell edge, with poor accuracy when the points were located at the ends, and therefore selected the Gauss points (nodes of a 2-point Gauss quadrature rule) as the MFIE test point locations for this comparison. The EFIE-D was point tested in the center of each face.

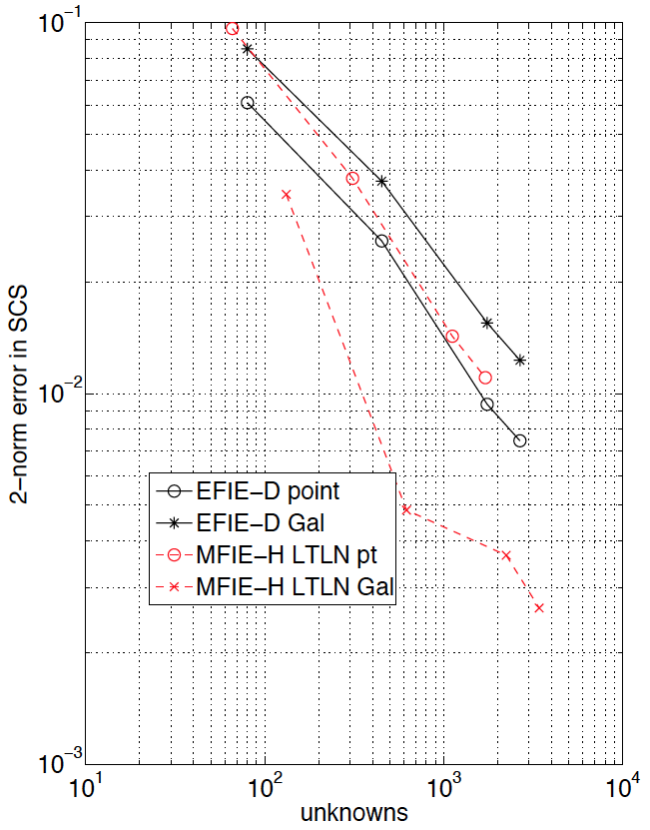

Fig. 9. The error in scattering cross section for a dielectric sphere with ka = 1.0 and ε_r = 5.

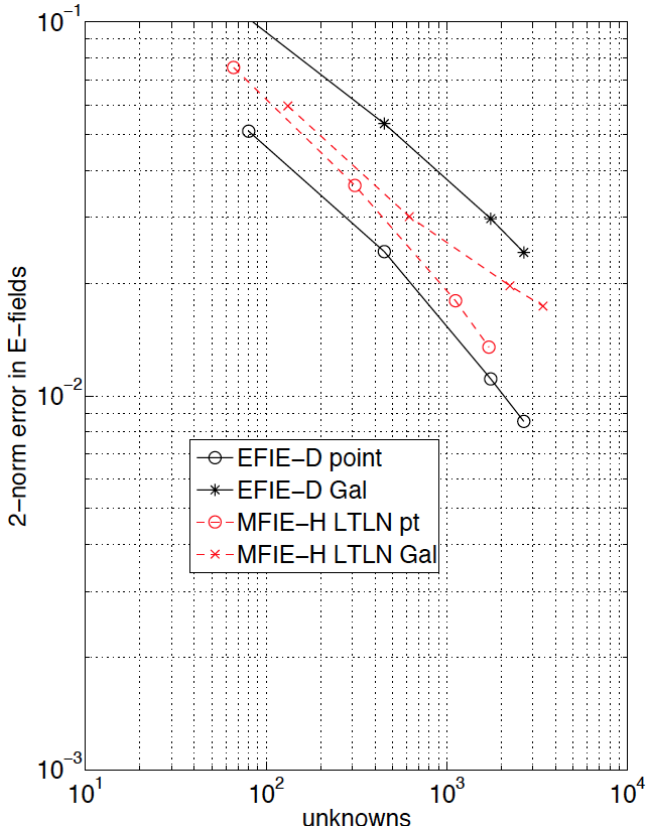

Fig. 10. The internal field error for a sphere with ka = 1.0 and ε_r = 5.

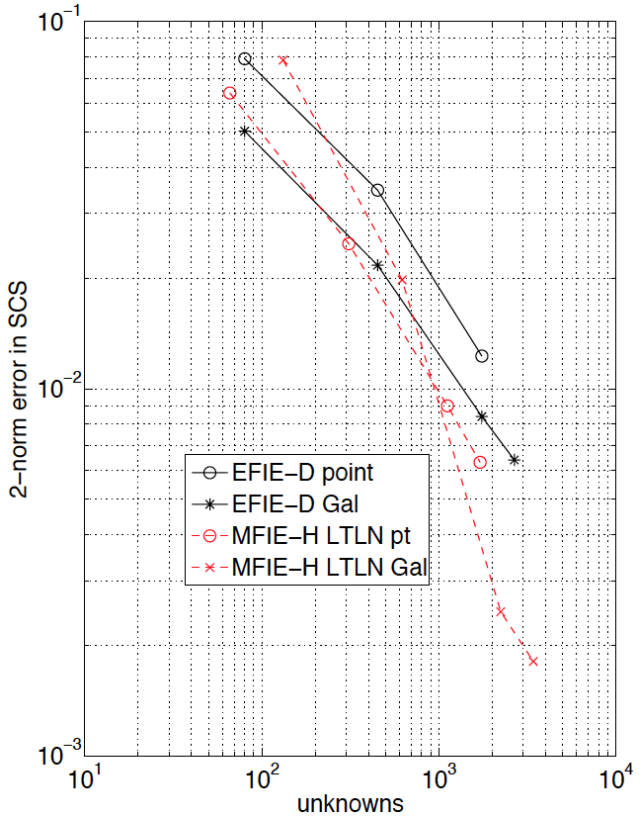

Fig. 11. The error in scattering cross section for a dielectric sphere with $ka = 0.35$ and $\varepsilon_r = 40 - j10$.

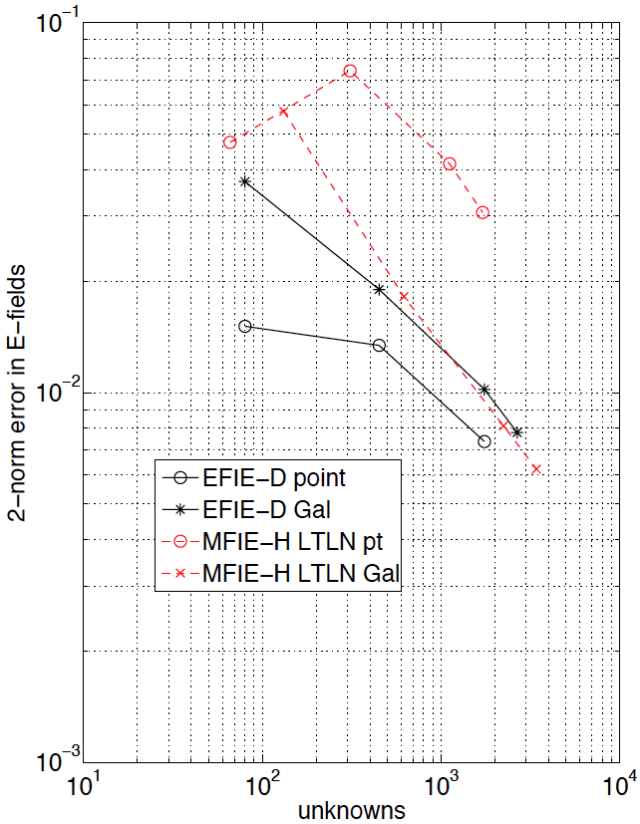

Fig. 12. The internal field error for a sphere with $ka = 0.35$ and $\varepsilon_r = 40 - j\,10$.

These preliminary results suggest that there is no consistent advantage in Galerkin testing for the EFIE-D. EFIE-D results obtained with point testing in Figures 9 and 10 are more accurate than those obtained with Galerkin testing, while the Galerkin results for scattering cross section in Figure 11 show a slight improvement over the point-tested results.

From an examination of these and other results (not shown) for the EFIE-D, we generally do not observe a faster convergence of the scattering cross section obtained with Galerkin testing relative to point testing. In other words, both testing schemes produce results that converge at an approximate $O(h^2)$ rate, where h is the average edge length of the mesh. (Since this is faster than the $O(h)$ rate of the interior fields, this suggests that the point-tested EFIE-D also produces superconvergent SCS results.)

In contrast, the MFIE-H results do show a definite advantage for Galerkin testing, even with twice as many unknowns as point testing. Results in Figure 9 show a substantial improvement in the accuracy of the SCS with Galerkin testing, and the SCS results in Figures 9 and 11 appear to converge at a faster rate than the $O(h^2)$ rate exhibited by the point-tested SCS. (Note that Figures 1, 3, and 7 did not show this accelerated convergence rate.)

Results from the MFIE-N approach, not shown, show an accuracy difference between point and Galerkin testing for SCS that is even greater than that exhibited by the MFIE-H LT/LN formulation (primarily due to the poor accuracy of the point-matched results when match points are placed at nodes of the mesh). If the match points are placed at the mesh nodes, the MFIE-H LT/LN produces the same SCS results as the MFIE-N. All results presented here for the point-tested MFIE-H LT/LN place the match points at the nodes of the 2-point Gauss quadrature rule along the edge, which always produced more accurate results than the edge endpoints. In any event, both linear basis MFIE approaches seem to produce superconvergent far fields when Galerkin testing is used, in accordance with theory [14]. For both point-tested MFIE approaches, and more commonly for the MFIE-N, we sometimes observe significantly larger errors in the internal electric fields with point testing than are produced by Galerkin testing. Figure 12 illustrates one such example.

VI. Conclusions and Questions

Three numerical discretization procedures for the volumetric EFIE and two for the volumetric MFIE have been investigated. (A sixth approach, the MFIE-H CT/LN, did not produce stable, converging results and was omitted from the comparison.) The EFIE-E and EFIE-H approaches are inherently Galerkin, while the others can be implemented with either point testing or Galerkin testing. Numerical results suggest that all five Galerkin formulations produce stable, converging numerical solutions for the far-zone scattering cross section and the internal electric fields. However, the computational efficiency of the approaches is quite different. The Galerkin EFIE-D formulation, a popular approach in widespread use,

requires the greatest number of unknowns for a given mesh and the greatest computational effort of any of the approaches to create the system of equations. For a given accuracy, the EFIE-H, MFIE-N, and MFIE-H LT/LN Galerkin approaches all appear to be consistently more efficient than the Galerkin EFIE-D. The author's interest stems in part from the use of fast direct solvers with volume integral equations, and therefore the performance of iterative solvers (and the related topic of matrix condition numbers) has not been investigated.

The point-tested EFIE-D formulation performed almost as well as the Galerkin-tested EFIE-D approach, suggesting that the additional effort being directed toward Galerkin testing for that formulation is usually wasted. The two Galerkin-tested MFIE formulations performed substantially better their point-tested counterparts, suggesting that the additional cost is worthwhile for the MFIE.

Various questions have arisen throughout the course of this study that bear further investigation: Why does the MFIE-H CT/LN formulation fail, while the MFIE-H LT/LN formulation works fine? Why is the point-tested EFIE-D approach as accurate as the Galerkin-tested EFIE-D, in contrast to similar approaches [19] applied to surface integral equations? Why is there sometimes a substantial improvement in the near fields (in contrast to the theory in [14]) when Galerkin testing is used with linear representations? (This behavior is also observed by the author with linear basis functions for both the EFIE and MFIE in two-dimensional problems [20], but not with constant or mixed-order basis functions.) Finally, why is the Galerkin EFIE-D so widely used, given that it is the most expensive approach and seldom as accurate on a per-unknown basis as the other available formulations?

REFERENCES

[1] D. E. Livesay and K. M. Chen, "Electromagnetic fields induced inside arbitrarily shaped biological bodies," *IEEE Trans. Microwave Theory Tech.*, vol. MTT-22, pp. 1273-1280, Dec. 1974.

[2] G. W. Hohmann, "Three-dimensional induced polarization and electromagnetic modeling," *Geophysics*, vol. 40, pp. 309-324, April 1975.

[3] D. H. Schaubert, D. R. Wilton, and A. W. Glisson, "A tetrahedral modeling method for electromagnetic scattering by arbitrarily shaped inhomogeneous dielectric bodies," *IEEE Trans. Antennas Propagat.*, vol. AP-32, pp. 77-85, Jan. 1984.

[4] A. F. Peterson, "A magnetic field integral equation formulation for electromagnetic scattering from inhomogeneous 3-D dielectric bodies," *Proc. 5th Annual Review of Progress in Applied Computational Electromagnetics*, pp. 387-403, March 1989.

[5] S. A. Carvalho and L. S. Mendes, "Scattering of EM waves by inhomogeneous dielectrics with the use of the method of moments and 3D solenoidal basis functions," *Microwave and Optical Technology Letters*, vol. 23, pp. 42-46, Oct. 1999.

[6] A. F. Peterson, "Efficient solenoidal discretization of the volume EFIE for electromagnetic scattering from dielectric objects," *IEEE Trans. Antennas Propagat.*, vol. 62, pp. 1475-1478, March 2014.

[7] R. A. Lemdiasov and R. Ludwig, "The determination of linearly independent rotational basis functions in volumetric electric field integral equations," *IEEE Trans. Antennas Propagat.*, vol. 54, pp. 2166-2169, July 2006.

[8] M. M. Botha, "Solving the volume integral equations of electromagnetic scattering," *J. Comp. Physics*, vol. 218, pp. 141-158, 2006.

[9] J. Markkanen, C.-C. Lu, X. Cao, and P. Yla-Oijala, "Analysis of volume integral equation formulations for scattering by high contrast penetrable objects," *IEEE Trans. Antennas Propagat.*, vol. 60, pp. 2367-2374, May 2012.

[10] L. E. Sun and W. C. Chew, "A novel formulation of the volume integral equation for electromagnetic scattering," *Waves in Random and Complex Media*, vol. 19, pp. 162-180, 2009.

[11] N. A. Ozdemir and J.-F. Lee, "A nonconformal volume integral equation for electromagnetic scattering from penetrable objects," *IEEE Trans. Magnetics*, vol. 43, pp. 1369-1372, April 2007.

[12] J. Markkanen, P. Yla-Oijala, and A. Sihvola, "Discretization of volume integral equation formulations for extremely anisotropic materials," *IEEE Trans. Antennas Propagat.*, vol. 60, pp. 5195-5202, Nov. 2012.

[13] P. P. Silvester and R. L. Ferrari, *Finite Elements for Electrical Engineers, 2nd Edition*. Cambridge University Press, 1990, p. 276.

[14] A. F. Peterson, D. R. Wilton, and R. E. Jorgenson, "Variational nature of Galerkin and non-Galerkin moment method solutions," *IEEE Trans. Antennas Propagat.*, vol. 44, pp. 500-503, April 1996.

[15] A. George and J. W. Liu, *Computer Solution of Large Sparse Positive Definite Systems*. Englewood Cliffs: Prentice-Hall, 1981.

[16] S. Pissanetzky, *Sparse Matrix Technology*. New York: Academic Press, 1984.

[17] O. Osterby and Z. Zlatev, *Direct Methods for Sparse Matrices*. (Lecture Notes in Computer Science 157). Berlin: Springer-Verlag, 1983.

[18] I. S. Duff, A. M. Erisman, and J. K. Reid, *Direct Methods for Sparse Matrices*. Oxford: Clarendon Press, 1986.

[19] A. F. Peterson, "Beyond RWG/Galerkin solutions of the EFIE: Investigations into point-matched, discontinuous, and higher order discretizations," *Proc. 27th Annual Review of Progress in Applied Computational Electromagnetics*, Williamsburg, VA, pp. 117-120, March 2011.

[20] A. F. Peterson, "Assessment of Galerkin testing for volume integral equations of electromagnetics," *Proc. 30th Annual Review of Progress in Applied*

Computational Electromagnetics, Jacksonville, FL, pp. 566-570, March 2014.

Andrew F. Peterson received the B.S., M.S., and Ph.D. degrees in Electrical Engineering from the University of Illinois, Urbana-Champaign. Since 1989, he has been a member of the faculty of the School of Electrical and Computer Engineering at the Georgia Institute of Technology, where he is now Professor and Associate Chair for Faculty Development. He has served as an Associate Editor of the *IEEE Transactions on Antennas and Propagation* and the *IEEE Antennas and Wireless Propagation Letters*, as the General Chair of the 1998 IEEE AP-S International Symposium and URSI/USNC Radio Science Meeting, and as a member of IEEE AP-S AdCom and the ACES Board of Directors. He is a past President of the IEEE AP-S and a past President of ACES. He is a Fellow of the IEEE, a Fellow of ACES, and a recipient of the IEEE Third Millennium Medal.